

## Application of Implicit 3D Modelling to Reconstruct the Layered Structure of the Comet 67P

Luca Penasa<sup>1</sup>, Matteo Massironi<sup>2</sup>, Emanuele Simioni<sup>3,4</sup>, Marco Franceschi<sup>2</sup>, Giampiero Naletto<sup>1,4,5</sup>, Sabrina Ferrari<sup>1</sup>, Ivano Bertini<sup>5</sup>, Pamela Cambianica<sup>3</sup>, Elisa Frattin<sup>3,5</sup>, Fiorangela La Forgia<sup>5</sup>, Alice Lucchetti<sup>3</sup>, Maurizio Pajola<sup>3</sup>, Frank Preusker<sup>6</sup>, Frank Scholten<sup>6</sup>, Laurent Jorda<sup>7</sup>, Robert Gaskell<sup>8</sup>, and Holger Sierks<sup>9</sup>

<sup>1</sup>University of Padova, Center of Studies and Activities for Space (CISAS) "G. Colombo," Via Venezia 15, 35131 Padova, Italy

<sup>2</sup>University of Padova, Department of Geosciences, Via G. Gradenigo 6, 35131 Padova, Italy

<sup>3</sup>INAF, Astronomical Observatory of Padova, Vicolo dell'Osservatorio 5, 35122 Padova, Italy

<sup>4</sup>CNR-IFN UOS Padova LUXOR, Via Trasea 7, 35131 Padova, Italy

<sup>5</sup>University of Padova, Department of Physics and Astronomy "Galileo Galilei," Via Marzolo 8, 35131 Padova, Italy

<sup>6</sup>Deutsches Zentrum für Luft- und Raumfahrt (DLR), Institut für Planetenforschung, Rutherfordstraße 23, 12489 Berlin, Germany

<sup>7</sup>Laboratoire d'Astrophysique de Marseille, UMR 7326, CNRS & Aix Marseille Université, 13388 Marseille Cedex 13, France

<sup>8</sup>Planetary Science Institute, 1700 East Fort Lowell, Suite 106, Tucson, AZ 85719, USA

<sup>9</sup>Max Planck Institute for Solar System Research, Justus-von-Liebig-Weg 3, 37077 Göttingen, Germany

### Abstract

We provide details about the procedure employed for the three-dimensional geological modelling of the lobes of comet Churyumov-Gerasimenko (67P). The two lobes of 67P are characterized by well visible terraces and elongated cliffs that revealed a pervasive layering arranged in an onion-like fashion. None of the layers can be traced for a continuity large enough to provide a means of stratigraphic correlation. Therefore, an explicit modelling approach of the layered structure is not easily applicable. We show how a very simple modelling strategy based on implicitly-defined analytical surfaces (spheres or ellipsoids), and requiring very limited operator decision-making, can be successfully applied to produce a geological model that easily fits the available scattered attitude observations. Our formulation has the advantage of providing a small set of parameters with a precise geometrical meaning that can be compared with other parameters of the lobes (i.e. center of ellipsoids and center of mass). The presented method originates outside commercial geological modelling software packages and required devising some ad-hoc solutions for the visualization of the resulting models in comparison with observations made on OSIRIS images. Some extracts of the visualization code, helpful for applying this procedure in similar operational contexts, are also presented.

### 11.1 Introduction

ESA's Rosetta spacecraft made it possible to observe the surface of the comet Churyumov-Gerasimenko (67P) at unprecedented resolution. The camera system onboard the spacecraft, the OSIRIS (Keller et al., 2007), captured tens of thousands of images during the two years of the mission, which were used for shape model reconstruction (Jorda et al., 2016; Preusker et al., 2017), spectrophotometric studies (Fornasier et al., 2015; Ockay et al., 2016), geomorphological mapping (Giacomini et al., 2016; Lee et al., 2016), and many other investigations on surface morphology and geology (El-Maarry et al., 2015a, 2016; Thomas et al., 2015; Birch et al., 2017; Vincent et al., 2017).

Comet 67P has a bilobate shape: the *big lobe* and the *small lobe* are connected through a bridge of material, known as the *neck* (see, for example, Sierks et al., 2015). The comet's nucleus is extremely rich in geomorphological forms. Among the most prominent ones are small- to large-scale fractures (El-Maarry et al., 2015b; Auger et al., 2017), landslides (Pajola et al., 2016) and morphological terraces. Terraces are flat portions of terrain, bounded on one or more sides by almost vertical cliffs: terraces and cliffs appear to be strongly associated and produce the whole range of intermediate morphologies between staircase-patterns of terraces to flat-topped *mesas*.

Terraces and cliffs are spatially organized, outlying a large-scale pervasive pattern of concentric and

semi-parallel layers (Thomas et al., 2015; Massironi et al., 2015; Rickman et al., 2015). This arrangement strongly recalls exposures of sedimentary and, less frequently, volcanic rocks observed on Earth and other rocky planets where the action of *differential erosion* enhances the original differences in the physical properties of the rocks. On comets the more prominent erosive process is expected to be sublimation (e.g. Keller et al., 2015; Guilbert-Lepoutre et al., 2015). Thus a process of *differential sublimation* might be a good candidate for explaining the terrace formation. The processes controlling terrace formation have produced a topographic profile of non-equilibrium, which alternates flat terrains with gravitationally failure-prone cliffs (Pajola et al., 2016). Figure 11.1, modified from Penasa et al. (2017a), shows the evidence for a tight alternation of terraces and cliffs on a typical topographic profile of 67P.

Terraces seem to form in correspondence of pre-existent extended surfaces, or bedding planes, which continue deep inside the nucleus. Terraces are observed for at least 1.2 and 1.38 km of stratigraphic thickness for the big lobe and the small lobe respectively, suggesting that a large portion of the cometary body is layered (Penasa et al., 2017a).

The same surfaces controlling the terraces can also be observed on vertical walls and inside pits, as linear traces produced by the intersection of the bedding planes with the surface (see, for example, Thomas et al., 2015; Massironi et al., 2015; Basilevsky et al., 2017). These traces are clearly aligned with nearby terraces and therefore represent the continuation of the terraces within the subsurface. No element contradicting this evidence has been found so far. While these traces are locally visible they cannot be followed for large distances, making the identification of key horizons difficult, and precluding any lateral correlation at the scale of the entire lobes. Their elusive appearance, which seems to be highly sensitive to the illumination condition (the same outcrop might show or not show

well-defined bedding planes, depending on the shadowing), suggests that these traces might actually be the result of small-scale terrace-like morphologies, at the limit with the image resolution.

In the next sections we will describe the process that led from the observation of terraces to a three-dimensional model of the layering. We will discuss the main problems related with such an uncommon case of a three-dimensional layered structure and how a working solution was obtained. The analytical solution described in this chapter was also used as a basis to create a more adaptive 3D model by Franceschi et al. (2020), where more details on this topic can be found.

### 11.1.1 From Terraces to Geological Cross-sections

The OSIRIS system is composed by two cameras: the Wide Angle Camera (WAC) camera with a larger field of view (FoV) of 12° and the Narrow Angle Camera (NAC) with a smaller FoV of 2.35°. Thanks to the large number of images collected during the Rosetta mission, three-dimensional meshes of the surface were produced by using either the stereophotogrammetry (SPG; Preusker et al., 2017) or the stereophotoclinometry method (SPC; Jorda et al., 2016). The models were produced incrementally by including new images in the reconstruction pipeline as they became available, so that the first generation of models comprised only the northern hemisphere of the comet.

From the analysis of the orientation of the terraces, Massironi et al. (2015) drew the first geological cross-sections of the inner layering, also showing that the terraces are aligned with the gravity equipotentials of each lobe taken individually, rather than being coherent with the gravity field of the entire bi-lobated nucleus. That evidence demonstrated the independent nature of the layering of the two lobes. To derive geological cross-sections

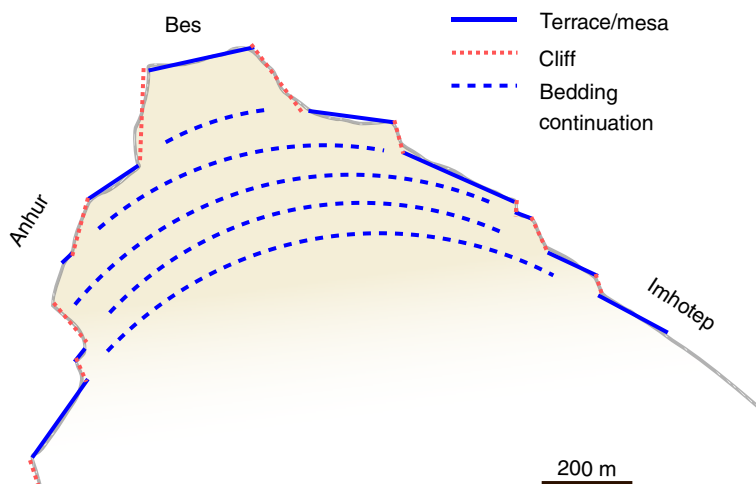


**Figure 11.1** A topographic profile obtained by cutting the shape model of Churyumov-Gerasimenko (67P) with a plane. Terraces and cliffs alternate, producing *staircase pattern* morphologies. Modified from Penasa et al. (2017a).

of the cometary nucleus, Massironi et al. (2015) estimated the orientation of the terrace on the 3D shape model that was available at the time, hence limited to the northern hemisphere of the Churyumov-Gerasimenko (67P) comet (Jorda et al., 2016) and characterized by a lower resolution. In particular, to estimate a best-fitting normal for each terrace surface, portions of the 3D shape model were extracted by using the meshlab software (Cignoni et al., 2008). The extracted vertices of the triangular mesh were then employed to obtain a best-fitting plane estimate of the terrace by means of a least squares method (e.g. Fernández, 2005).

From the three-dimensional shape model a set of cross-sections were extracted providing topographic profiles of the comet nucleus. A subset of the obtained terraces, located within a buffer from the section plane, was then plotted on the same cross-section to represent the local orientation of the layering. From this information, Massironi et al. (2015) interpreted the inner layering as formed by extended surfaces, whose intersections with the two-dimensional section were traced by respecting the orientation imposed by the terraces. A similar methodology was employed for drawing geological cross-sections used during planning of the Brenner basis tunnel (Bistacchi et al., 2008; Schiavo et al., 2015).

This approach provided geological sections like the one in Figure 11.2, in which the terraces, interpreted as proxies for the underlying bedding planes, are extended inside

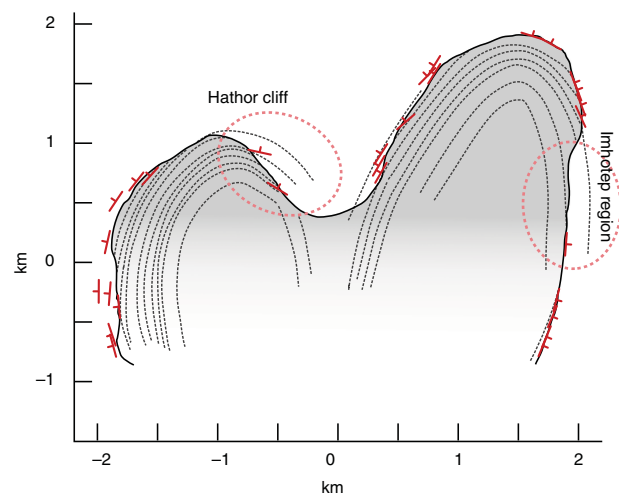


**Figure 11.2** One of the geological cross-sections realized by Massironi et al. (2015), redrawn and simplified. Red marks represent the measured orientations at the section plane of the observed terraces and their normals. Dashed lines are the interpreted continuation of the terraces as extended bedding planes inside the nucleus, which were traced in accordance with the observed attitudes at the surface. On some regions the stratigraphic series is well exposed for some hundreds of meters of the total thickness (dotted ellipses).

the nucleus. This provided an indication not only about the expected orientation of the layers below the surface but also about the overall layered sequence thickness, which was shown to be of the order of hundreds of meters. Although being limited to the northern hemisphere, this analysis showed that large portions of the layered sequence were actually missing, for example on the Hathor cliff, where the layers meet the topographic surface at a high angle (Figure 11.2).

To better constrain the geometry of the layers, the creation of a three-dimensional model was of primary importance. A typical workflow for producing three-dimensional models of sedimentary sequences involves the creation of a set of cross-sections on which the subsurface continuation of layers/horizons is tracked and/or interpreted. As layers are intersected by each cross-section in depth, it is possible to create surfaces fitting the traces of each layer in three dimensions. This approach is defined as *explicit modelling* (Caumon et al., 2009). Although cross-sections of Churyumov-Gerasimenko (67P) were readily available (at least for the northern hemisphere) from Massironi et al. (2015), the creation of a explicit model turned out to be a difficult task. Using 67P it is not possible to clearly identify any stratigraphic key horizon that could be identified and traced on all the cross-sections. This makes it difficult to establish a sure lateral continuity of the strata over a couple of hundred meters. Indeed, on 67P only scattered attitude information exists, and hence each geological section can be internally self-consistent with the nearby strata attitudes but there is no objective way to establish the stratigraphic correlation among different sections (see Figure 11.3). Although it would in principle be possible to solve this problem by explicitly correlating the layers on different sections, any resulting model would be highly interpretative and subject to the choices enforced by the operator performing the modelling.

The 67P case indeed highlights the severe limitations of generating 3D models from two-dimensional cross-sections when little or no information about the stratigraphic sequence is available.

## 11.2 A Modelling Strategy for Onion-Like Layers

Three-dimensional modelling strategies in geoscience can be grouped into two categories: *implicit* or *explicit* (e.g. Rolo et al., 2017). In the *explicit* approach, the surfaces are constructed as meshes and modified through direct interaction with their geometrical parameters. In the *implicit* approach, instead, surfaces are constructed as iso-potential surfaces of a scalar field. The first method

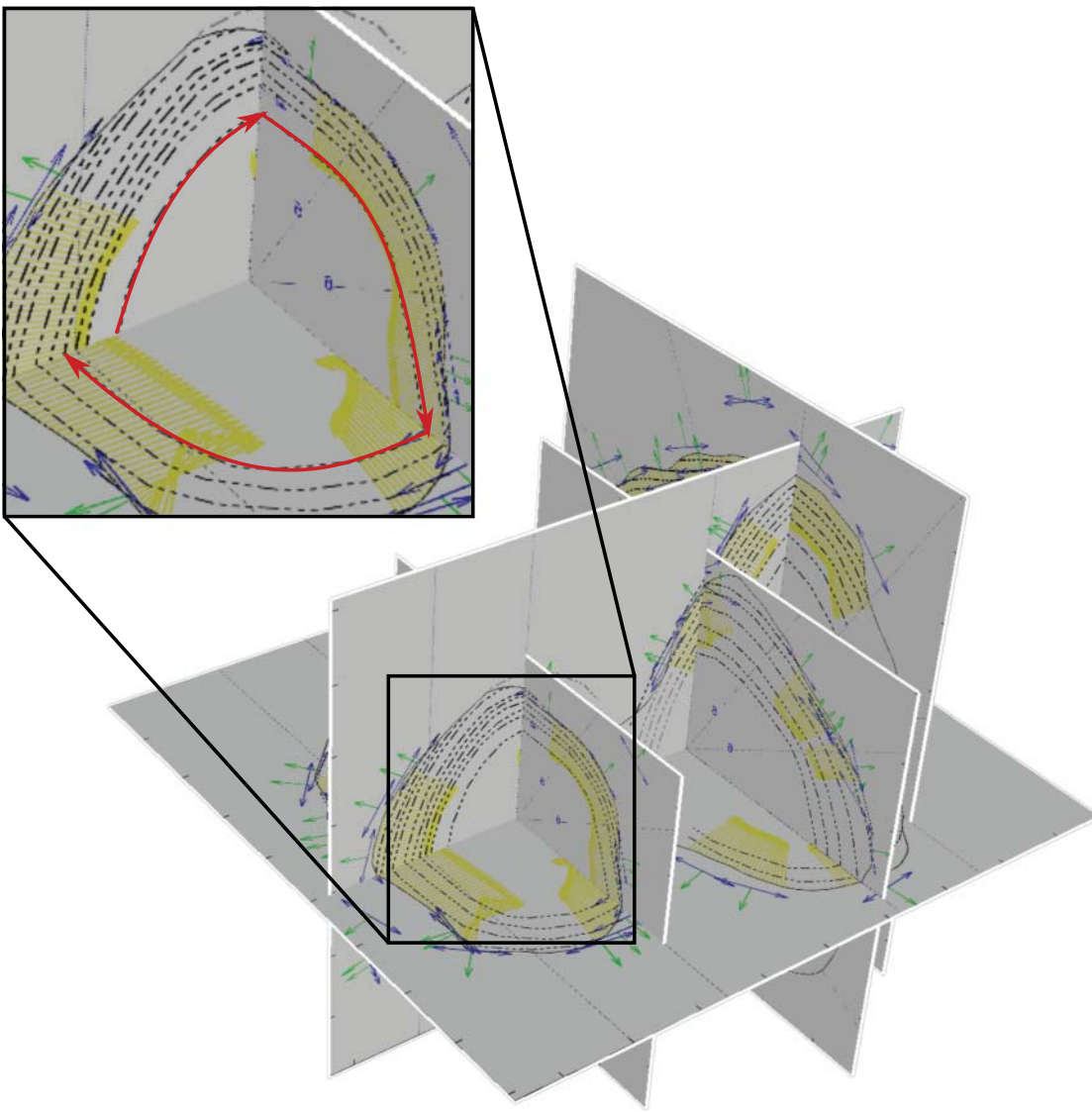


**Figure 11.3** The geological cross-sections realized by Massironi et al. (2015) imported and aligned within *GoCAD/SKUA*® 3D geological modelling software: the sections provide a framework for the generation of an explicit interpretation, but the absence of any clear stratigraphic marker that could be extended throughout all the sections does not allow an explicit approach to be strictly followed. The top frame highlights the inconsistencies that are introduced when trying to correlate layers on different sections that were independently realized.

works better when good constraints (e.g. in the form of key horizons) are available but it proved not to be well suitable for comet 67P as the explicit creation of bedding planes would have required the identification of lines and terraces well correlated at the scale of the entire comet (i.e. terraces belonging to an original continuous or semicontinuous bedding plane of global extension). Such correlation, as already noted, could not be done on 67P without involving a series of assumptions not supported by clear evidence.

An *implicit* modelling approach (see, for example, Hillier et al., 2014; Calcagno et al., 2008; Grose et al., 2021) was

thus pursued to obtain a simplified numerical representation of the layered sequences of Churyumov-Gerasimenko (67P) lobes. Implicit models seek a representation of a specific layer as a contour surface of a three-dimensional, real-valued function  $f$ :

$$f(\mathbf{p}) = f_1 \quad (11.1)$$

where  $f_1$  is a scalar associated with a specific layer and  $\mathbf{p} = [x, y, z]^T$  is a point part of it. Function  $f$  should ideally represent the *stratigraphic position* (a value representing the position of a point in the stratigraphic pile) of any given three-dimensional point. The modelling function

$f$  is normally an interpolator that satisfies some a-priori constraints, typically related to the smoothness of the generated surfaces. Several different interpolation algorithms have been proposed, mostly based on Radial Basis Functions (RBFs) (Hardy, 1990), kriging (Hardy, 1990), or *discrete* interpolants (Caumon et al., 2013). Although interpolation-based modelling schemes are extremely adaptive and can be used to represent highly complex geological bodies (e.g. mineralization ores), the parameters of the models lack a concise physical meaning, making it more difficult to interpret the results of the modelling.

For these reasons we made use of the knowledge about the layering on 67P lobes, to formulate an ad-hoc modelling function. The terraces, and hence the layering, appear to be geometrically aligned to the gravity equipotentials of each lobe (Massironi et al., 2015), thus suggesting that a roundish shape could be well representative of the layers.

A simple spherical modelling (SP) function in three dimensions can be constructed as follows (see Figure 11.4):

$$f(\mathbf{p}) = \|\mathbf{p} - \mathbf{c}\| \quad (11.2)$$

This kind of implicit function predicts the stratigraphic position of any point  $\mathbf{p} = [x, y, z]^T$  as a distance from a center  $\mathbf{c} = [x_0, y_0, z_0]^T$ . Such a simple model represents each layer by a spherical surface, centered on the point  $\mathbf{c}$  (see the two-dimensional example in Figure 11.4). Notice that in this case the gradient of the function at any given point is always unitary:

$$\|\nabla f(\mathbf{p})\| = 1 \quad (11.3)$$

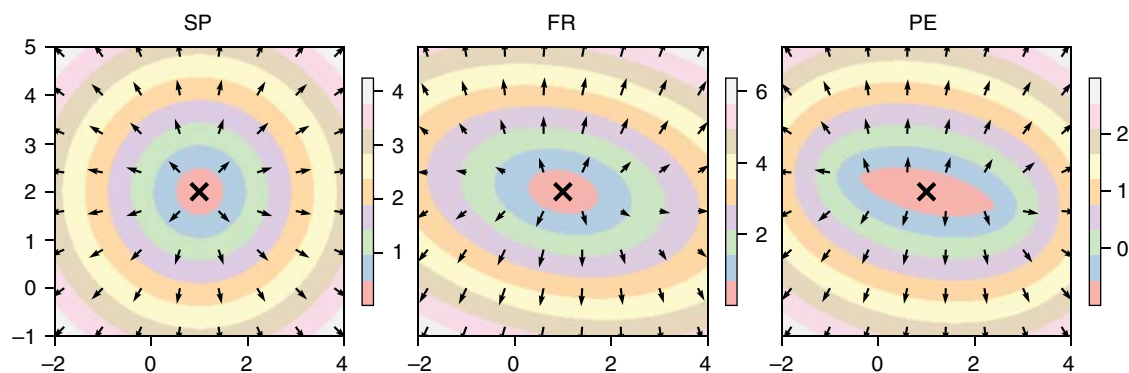


**Figure 11.4** Three different modelling functions for roundish concentric layers. A simple modelling function (SP) can be defined as the distance from a point. Contour lines (or surfaces in 3D) can then be traced and used to represent concentric shells. The gradient at any given point (arrows) provides a means of estimating the local orientation of the layers, which can be compared with measured orientations (the observed orientations of terraces). The layers for an FR model (concentric ellipsoids with fixed axial ratios) are not parallel to each other, which is a common requirement in geological modelling. This issue can be solved with the Parent Ellipsoid (PE) model (distance field from a parent ellipsoid), but this would produce unrealistic lens-shaped layers in the interior of the parent ellipse (or ellipsoid in 3D). In this example units are arbitrary.

Hence this kind of model represents a real metric of distance (being defined as such) in the depth space: if we consider two different layers at  $f_1$  and  $f_2$  we can compute the thickness of the comprised layering as the difference of the scalar field between the two ( $f_1 - f_2$ ).

The modelling strategy based on spherical shells can also be adapted to other analytical shapes. To derive a modelling function that could account for the evident non-sphericity of the lobes of 67P we made use of ellipsoids: Figure 11.4 illustrates this concept in two dimensions. A first possibility consists in using a family of concentric ellipsoids sharing the same axial ratios (Fixed axial Ratios model, hereafter FR). The obtained modelling function (see also Penasa et al., 2017a) is

$$f(\mathbf{p}) = g(\mathbf{R}^T \cdot (\mathbf{p} - \mathbf{c})) \quad (11.4)$$

and the relative gradient is

$$\nabla f(\mathbf{p}) = \mathbf{R} \cdot \nabla g(\mathbf{R}^T \cdot (\mathbf{p} - \mathbf{c})) \quad (11.5)$$

where the function  $g(\mathbf{p})$  is defined as

$$g(\mathbf{p}) = \frac{1}{bc} \sqrt{b^2 c^2 x^2 + b^2 z^2 + c^2 y^2} \quad (11.6)$$

The rotation matrix  $\mathbf{R}$  represents the orientation of the ellipsoidal shells in space, and can also be parametrized as three angles  $\alpha, \beta, \gamma$  (yaw-pitch-roll), while  $\mathbf{c}$  is the common center of the ellipsoidal shells. The parameters  $b$  and  $c$  are the axial ratio of the ellipsoidal family and  $x, y, z$  are the coordinates of any point  $\mathbf{p}$ . This choice provides a modelling function that has a simple analytical expression but has the drawback of producing ellipsoidal shells that are not parallel to each other; thus the thickness of the layers is variable (see Figure 11.4, FR model).



On the other hand, a model in which thickness is preserved (Parallel Ellipsoids model, hereafter PE) can be obtained by defining the function  $f(\mathbf{p})$  as the distance from a *parent ellipsoid*, which can be defined by its  $a, b, c$  parameters,  $\mathbf{R}$  and  $\mathbf{c}$  (see also Laurent, 2016, for a discussion on thickness preservation when dealing with discrete implicit models). This kind of model thus requires the *distance* from an ellipsoid to be computed, a problem that does not have an analytical solution and has to be solved numerically by finding the zeroes of a sixth degree polynomial. A *robust* algorithm is described in Eberly (2013) and its implementation can be found in the *Geometric Tools* repository ([www.geometrictools.com](http://www.geometrictools.com)). This type of model, which would have the desirable property of having a unitary gradient everywhere, has the serious drawback of producing unrealistic lenticular shapes inside the parent ellipsoid (see the two-dimensional representation of Figure 11.4, PE model).

Table 11.1 summarizes some simple models that can be used for modelling onion-like layered bodies. All these models can find application when modelling roundish layered bodies, although an SP model can be too simple to approximate complex shapes well. For solving this issue an FR or PE model can be used to obtain a more adaptive shape, although the FR model has better properties in term of the resulting shapes (no lens-shaped shells inside the parent ellipsoid) and it is simpler to implement, having an analytical solution for the function value and its gradient. This function has the only drawback of not being thickness-preserving, but it might be acceptable if there are not strict reasons to impose this constraint, as in the case of 67P, where continuous layers of constant thickness have not been observed.

As a side note, we highlight the fact that the implicit formulation of these models simplifies their use as “base models” for other implicit modelling techniques: if the object to be modelled deviates locally from the base shape (e.g. the ellipsoid), additional implicit functions (e.g. RBF) can be used to account for residuals by just summing the

contribution of the base-shape implicit model with a more adaptive one. For example, an extended model  $f'(\mathbf{p})$  could be obtained as

$$f'(\mathbf{p}) = f(\mathbf{p}) + r(\mathbf{p}) \quad (11.7)$$

and the gradient as

$$\nabla f'(\mathbf{p}) = \nabla f(\mathbf{p}) + \nabla r(\mathbf{p}) \quad (11.8)$$

where  $f(\mathbf{p})$  is any of the SP, FR, or PE models, and  $r(\mathbf{p})$  is another, more flexible, interpolator (e.g. RBF or kriging) that could be used to take into account the deviations from the base shape.

### 11.3 Model Fitting

The parameters of the model must be determined by maximizing the agreement between predictions and observations. In this case, each observation is a point in space  $\mathbf{p}_i = [x, y, z]^T$  associated with a unit vector  $\mathbf{n}_i = [nx, ny, nz]^T$  representing the direction perpendicular to the layers at that location, as depicted in Figure 11.5. The available data does not provide any direct observation of the scalar field to be modelled (values of the function  $f$ ), but only of its normalized gradient  $\mathbf{n}_i$ , which can be compared with the predicted gradient as an angular measure:

$$\theta_i = \arccos\left(\frac{\nabla f(\mathbf{p}_i)}{\|\nabla f(\mathbf{p}_i)\|} \cdot \mathbf{n}_i\right) \quad (11.9)$$

By minimizing these angles via a non-linear least-squares solver, the best-fitting parameters for any selected  $f$  model can be found. We made use of the CERES C++ package (Agarwal et al., 2016) to develop a simple toolkit for fitting implicit models. Each model requires the definition of two methods: one for computing the value of  $f(\mathbf{p})$  and one for its gradient  $\nabla f(\mathbf{p})$ , and can then be easily fitted to any dataset of observations. Alternatively to unit normals, polylines describing the edges of the terraces could also be used to constrain the model, with just minor changes to the fitting strategy of Equation (11.9). More information on this approach can be found in Ruzicka et al. (2019).

In the case of the fixed-ratios ellipsoidal model (FR) the parameter vector can be written as

$$\mathbf{x} = [c_x, c_y, c_z, b, c, \alpha, \beta, \gamma]^T \quad (11.10)$$

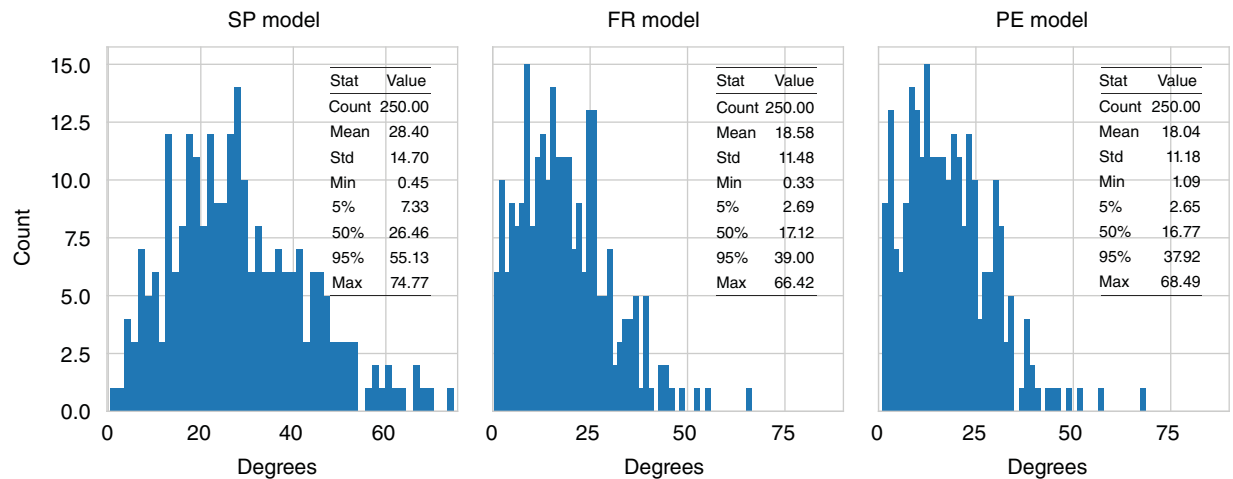
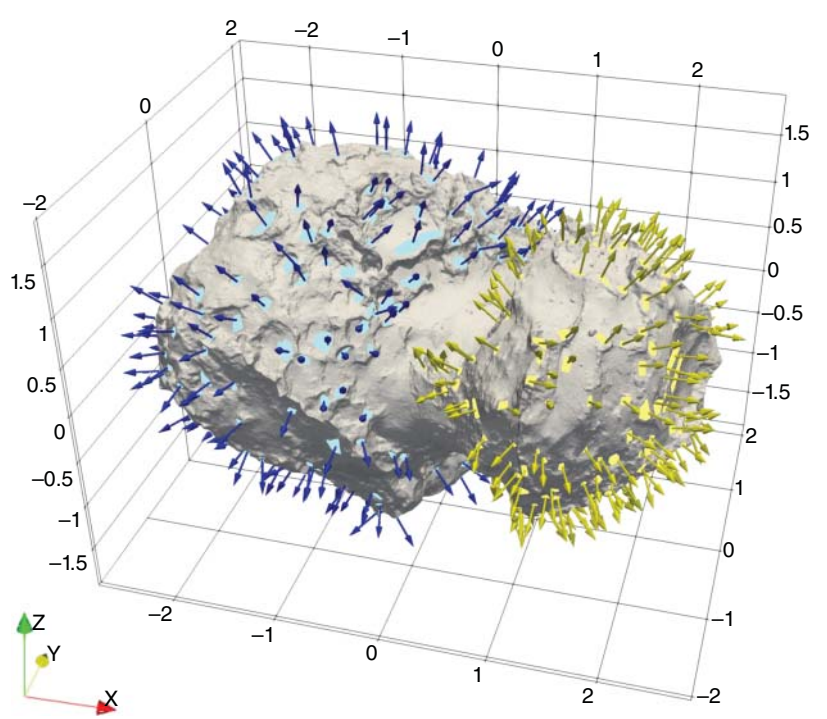
Given a set of initial values, the solver finds the vector of parameters that minimizes the angular residuals of Equation (11.9).

Figure 11.6 shows the histograms of the best-fitting model residuals in the case of the spherical model (SP), the fixed ratios model (FR), and for a model based on shells

**Table 11.1** Some of the functions that were tested as a modelling function for the layers of 67P lobes.

Abbreviation	Function	Number of parameters	Analytical solution
SP	Spherical	3 (x,y,z)	Yes – very simple
FR	Fixed ratios	3 (x,y,z) + 2 (b,c) + 3 (α, β, γ)	Yes – very simple
PE	Parallel Ellipsoid	3 (x,y,z) + 3 (a,b,c) + 3 (α, β, γ)	None

**Figure 11.5** The 3D shape model of Churyumov-Gerasimenko (67P) (Preusker et al., 2017; Jorda et al., 2016). Each arrow represents an observation used as a constraint to model the layers. These attitudes were obtained by selecting a portion of the 3D model representative of terraces. A best-fitting procedure on selected vertices provided a unit normal perpendicular to each terrace. Colored patches correspond to the portions of the shape model that were used for the plane fitting.



**Figure 11.6** Histograms and statistics for the angular residuals for three different best-fitting models for the Big Lobe of comet 67P. In the case of the spherical model (SP), each layer is approximated by a concentric sphere. A family of ellipsoids with fixed axial ratios (FR) provide similar average residuals as the one based on parallel shells (PE). The FR model is simpler to implement and avoids the creation of lens-shaped shells within the parent ellipsoid. The average residuals is of  $\sim 10^\circ$  smaller using the PE ellipsoidal model, with respect to the simpler spherical one, where almost no residuals below  $10^\circ$  are present.

parallel to a parent ellipsoid (PE). The FR model was used in Penasa et al. (2017a) and was chosen to be the *reference* model for the layers on 67P because it provided a residual comparable to the PE model with the additional benefit of not producing the inner lenticular shapes that can be observed in Figure 11.4. The residuals can be also evaluated for their location on the cometary body. Figure 11.7 shows each observation as a vector in space, colored by the angular residual of the model at that location. Observations

with higher residuals does not cluster in specific locations, but are rather well-scattered on the whole body, suggesting that they can mostly be considered as outliers, rather than deviations of the layers from the ellipsoidal shape that was employed.

In the case of an FR model, three parameters are needed to define the center of the ellipsoid, while  $b$  and  $c$  are the axial ratios of the ellipsoidal shells and  $\alpha$ ,  $\beta$ ,  $\gamma$  are *yaw*, *pitch*, and *roll* angles, defining their orientation in space.

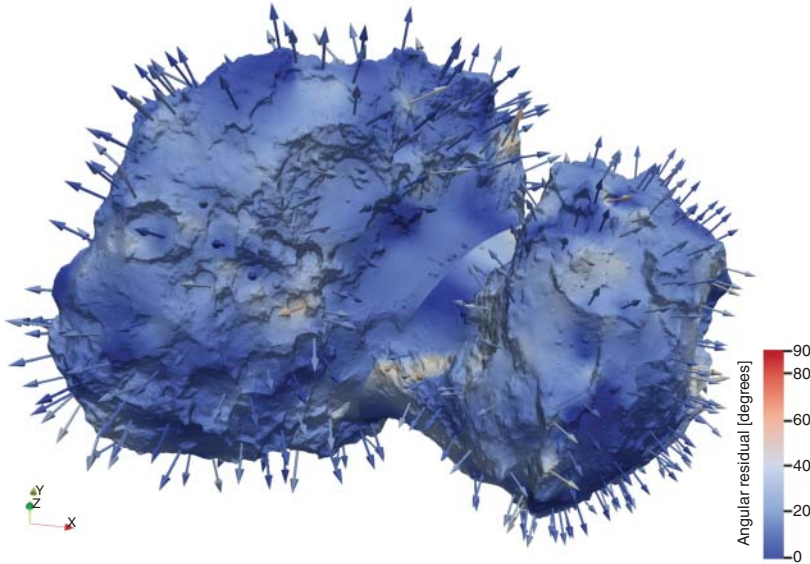


**Figure 11.7** The angular residuals resulting from the model can be visualized by mapping the angles to a color scale (0° to 90°) and using them to color the vectors representing the observations. In this case (the best-fitting FR model), the residuals have been also interpolated on the surface for visualization purposes.

The management of the angular parameters  $\alpha$ ,  $\beta$ , and  $\gamma$  requires some special attention during implementation because an ellipsoid has three symmetry axes and thus different triplets of angles might actually represent ellipsoidal models with an equivalent orientation in space. As an example, consider a generic triaxial ellipsoid: a rotation of 180° around any axis produces an ellipsoidal model that is equivalent for the scope of our modelling to the one in the non-rotated state.

Also, the  $a$ ,  $b$ , and  $c$  parameters require a similar care. These parameters are often constrained in this way:

$$a \geq b \geq c > 0 \quad (11.11)$$

Although several non-linear optimization packages allow the solution to be constrained by defining the bounds for each parameter, we found that this strategy could be counter-productive, slowing down or preventing convergence. A working solution consists in letting the solver reach convergence through the more convenient path in the parameters space, for example by providing a solution of the kind  $b \geq c \geq a > 0$ , which can be easily reformulated in the expected form by reordering the columns of the orientation matrix  $\mathbf{R}$  and the respective values of the semi-axis.

When determining parameters by nonlinear methods, it is important to initialize the vector of parameters with values that are *near* the global minimum, to have faster convergence and possibly avoid local minima. The overall topography of the object can be used as a first approximation of the shape of the layers and thus the center of the model can be set to match the centroid of the observations. Initializing the orientation and the axial parameters might be more complex and can be, for example, obtained by Principal Component Analysis (PCA) applied on the locations of the observations.

### 11.3.1 Errors Determination

To associate an error to each model's parameter, a *bootstrap* method based on a Monte Carlo resampling (Efron, 1979; Chernick, 2008) has been applied. The method can be implemented in the following iterative way:

1. A new dataset of observations is generated by resampling with replacement of the original dataset. This simulates the effect that might be introduced by a new data-collection campaign.
2. The best-fitting solution is determined as described above, and the vector of the best-fitting parameters is stored.

These two steps are repeated for a large number of times (i.e. 10,000), thus providing a new best-fitting solution at each iteration. We found that in the specific case, when fitting an FR ellipsoidal model, even starting with a naive initialization of the parameters (i.e. the center located in the centroid of the observations, randomly chosen axial ratios in between 0.6 and 1.0, and axes aligned with the Cartesian axes of the reference frame), the rate of convergence resulted in 100% (all iterations converged properly).

The bootstrap method provides a large number of parameter vectors for the chosen model, which can be summarized as histograms. As an example, Figure 11.8 shows three histograms for each lobe representing the coordinates of the FR ellipsoidal model center. The histograms exhibit well-shaped Gaussian distributions, suggesting that the parameters converge toward the same solution: this makes the hypothesis of multiple solutions for the considered model unlikely. From these distributions it is possible to obtain the maximum likelihood solution, while the associated standard errors can be obtained by statistical



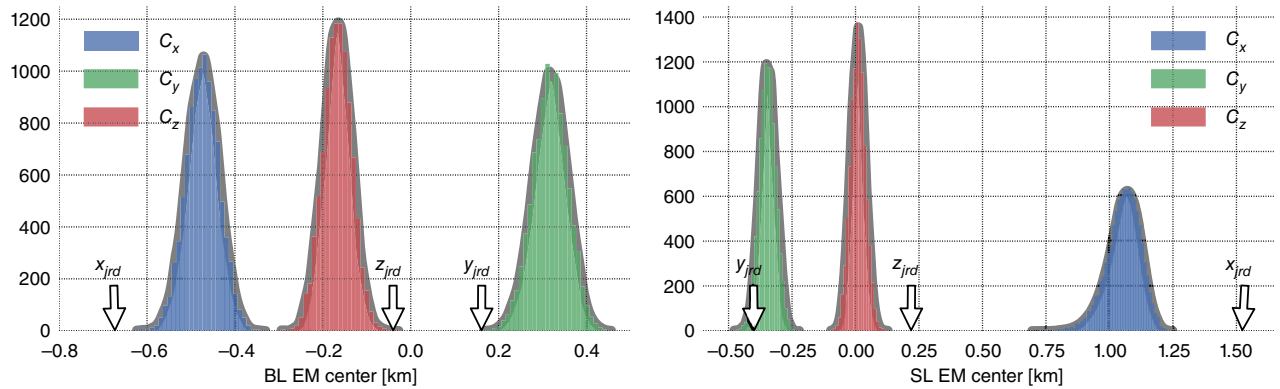


**Figure 11.8** Distributions of the ellipsoidal model center  $[c_x, c_y, c_z]$  resulting from the bootstrap iterations. The coordinates for the center of mass computed by Jorda et al. (2016) are reported with the *jrd* subscript.

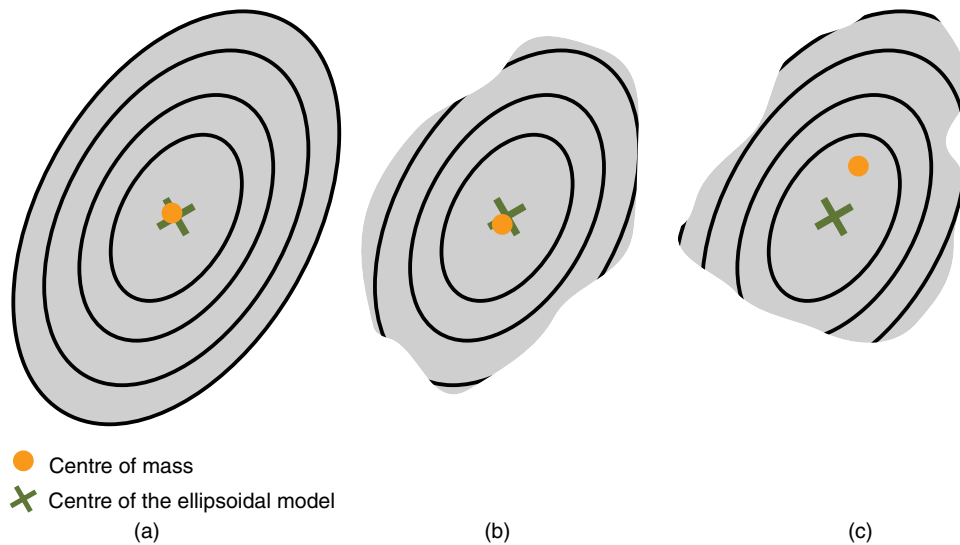


**Figure 11.9** The center of mass of the modelled lobe would be expected to correspond to the center of the ellipsoidal model whenever the object is (a) intact or (b) when it underwent an approximately homogeneous erosional process. In the case of localized material removals, the center of mass is expected to be significantly shifted (c), as was in fact observed for comet 67P (Based on Penasa et al., 2017a).

means, taking care to use circular statistics for the angles (Fisher, 1993). A complete table of the parameters and their errors, as determined by the described procedure assuming an FR ellipsoidal model, can be found in Penasa et al. (2017a). We will limit the discussion here to the coordinates of the center of the ellipsoidal models.

The proposed modelling strategy has the advantage of providing a set of parameters with an unambiguous geometrical meaning and may help to provide quantitative/semi-quantitative measurements useful to the study of the comet. For instance, the *center*  $[c_x, c_y, c_z]$  of the ellipsoids can be compared with the center of mass of the respective lobe. Assuming a homogeneous density of the nucleus, the center of the ellipsoidal model and the center of mass of the lobe are expected to coincide. Any deviation from this configuration might suggest that the

lobe underwent a localized erosional process that removed more material in specific locations. Figure 11.9 illustrates this concept.

In the case of 67P this analysis revealed that the center of mass in both cases does not coincide with the center of the respective ellipsoidal models. Table 11.2 reports on the center of mass for the two lobes of 67P, which are also displayed in Figure 11.8 as white arrows.

We found that the two centers of mass are significantly shifted with respect to the centers of the FR ellipsoidal models, by about 300 and 500 meters for the big and the small lobe respectively. To evaluate whether these values are significant or not, the estimated errors must be considered. The center of mass was computed by considering a homogeneous density for the material and, under this assumption, the error can be considered as negligible when

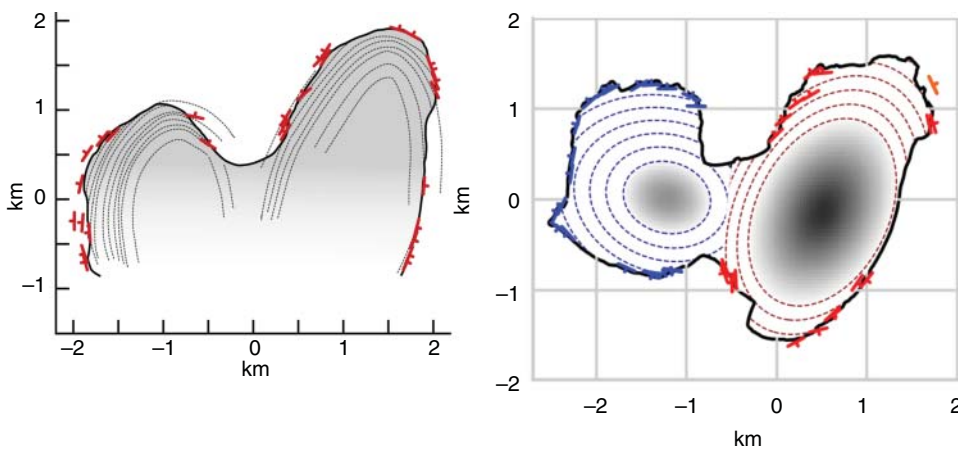


**Figure 11.10** Comparison of a cross-section. On the left, the section number 4, from Extended Data Figure 8 by Massironi et al. (2015), was obtained by interpretation of orientation data. The one on the right was obtained from the ellipsoids-based FR model by Penasa et al. (2017b).

**Table 11.2** Center of mass of the lobes, as computed by Jorda et al. (2016), compared to the center of the FR model from Penasa et al. (2017a).

	Center of mass	Center of FR model
Big lobe	$[-0.673, 0.147, -0.049]$ km	$[-0.473, 0.320, -0.167]$ km
Small lobe	$[1.524, -0.391, 0.208]$ km	$[1.060, -0.346, 0.010]$ km

compared to the standard errors for the centers of the FR ellipsoidal models. When these values are compared with the distributions of the ellipsoidal model parameters (see Figure 11.8), it appears evident that there is a consistent shift of the coordinates (well above the significance level), especially along some directions. For example, the  $x$  coordinate of the center of the FR ellipsoidal model for the small lobe is shifted by about 500 meters. This shift can be ascribed to the large volumes of cometary material, which are missing on the Hathor cliff (see Figure 11.2). The statistically significant differences between the centers of mass and the center of the respective ellipsoidal models thus support the idea that the nucleus underwent significant processes of uneven material removal (see Figure 11.9).

## 11.4 Visualization and Validation of the Models

Once the most likely ellipsoidal model is found through the described bootstrap method, it is necessary to convey the model so that it can be used to validate the geological interpretation. The simplest approach consists

in generating a series of geological cross-sections of the model. Figure 11.10 shows the comparison of two sections obtained from the FR most-likely model and the original section by Massironi et al. (2015). The obtained section is now granted to be consistent with any other section that could be generated from the model. This picture also highlights the great improvements that were obtained for the 3D shape model of 67P during the years of the mission.

Alternatively, a certain number of ellipsoidal shells of the model can then be overlaid in any 3D visualization software. Although this approach gives the precise idea of the geometry of the used model, it does not allow the model to be easily compared with other information because the shells tend to occlude the view, even if some transparency rendering is employed. In particular, the obtained model is expected to produce shells that, once intersected with the local topography, should be parallel to nearby terraces following the related scarps.

For this reason we used the modelling equation (i.e. Equation (11.4)) to compute the scalar value of the ellipsoidal model function  $f(\mathbf{p})$  for each vertex of the shape model, thus providing a scalar field that can be easily visualized thanks to the ParaView software (Squillacote et al., 2007) by mapping the values to a color scale (Figure 11.11a). The scalar values computed using Equation (11.4), in the case of an ellipsoidal model with fixed axial ratios, correspond to the value of the semimajor axis of the ellipsoidal shell passing for that location (hence its name, Reference Ellipsoid Semimajor axis, or simply RES). ParaView is an open source software for scientific visualization built on top of the VTK library (Schroeder et al., 2006) and can be used to visualize three-dimensional mesh models and the associated scalar fields (scalar values associated with the vertices or the facets of the models).

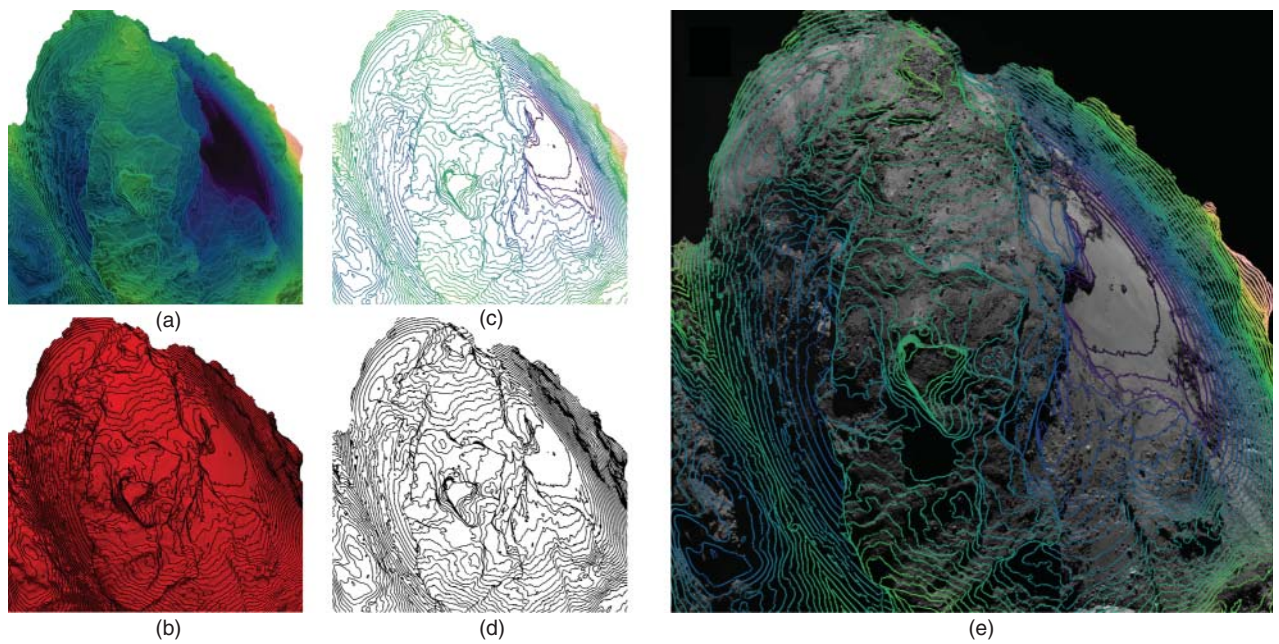


**Figure 11.11** To overlay the RES contour lines on a real OSIRIS image, the geometry of the shape model must be taken into account. This can be done by (d) creating a mask and (b) using an ad-hoc color mapping. The mask can then be used to extract the contour lines from (a) to obtain the color contour-lines image, as shown in (c). These can then be easily overlaid to any NAC or WAC image (e). (ImageID reference NAC\_2016-01-27T16.27.58.970.)

The primary source of information used in this work is the collection of images generated by osiris, thus comparing the modelling results with any NAC or WAC image (Figure 11.11a) is of primary importance. To correctly overlay ParaView-generated images with OSIRIS images, we created a Python script to align the camera to the NAC or the WAC cameras, by using the information provided by the mission's SPICE kernels (<https://www.cosmos.esa.int/web/spice/spice-for-rosetta>) (Acton et al., 2018). Retrieving the camera's orientation and position with respect to 67P can be done in Python by using the spiceypy toolkit (Annex et al., 2017):

```
import os
import spiceypy

# load the spice kernels
os.chdir("cgkernels/mk/")
spiceypy.furnsh("ROS_V111.TM")

# the time at which the camera position is needed
t = "2016-01-27T16:27:58.970"
# transform the string to a time
t = spiceypy.str2et(t)

# get the position of Rosetta spacecraft in 67p
# reference frame,
# centered in 67P, no light time correction
center = spiceypy.spkpos("ROSETTA", t,
"67P/C-G_CK", "NONE", "67P/C-G")[0]
```

```
# rotation matrix of the NAC camera,
# in respect to 67P reference frame
Rot = spiceypy.pxform("ROS_OSIRIS_NAC",
"67P/C-G_CK", t);
```

The variables center and Rot correspond to the optical center and the rotation matrix of the camera, and can be used to align the view of ParaView with the NAC or WAC camera at the time  $t$ . The code first obtains the rotation matrix and the position vector as above, then resets the current camera position to a known one, and finally applies the transformation matrix build by using the variables center and Rot. This strategy can be easily scripted to process a large number of camera's positions and to automatically obtain matching screenshots for any number of NAC or WAC images.

```
# and the active camera
camera = GetActiveCamera()
view = GetActiveView()
view.CameraParallelProjection = 0

# get center and rotation of camera
center, Rot = getNacCenterAndRotationAtTime(t)
# as above
# we create a homogeneous transformation matrix,
# embedding center and rotation
Rt = np.zeros((4,4))
Rt[3,3] = 1
Rt[:3,:3] = Rot
Rt[:3,3] = center
```

```

# we do a total reset to start in a known
  position
camera.SetFocalPoint(0, 0, 1)
camera.SetPosition(0, 0, 0)
camera.SetViewUp((0, 1, 0))
camera.SetRoll(-90)
camera.SetWindowCenter(0, 0)

# create a transform
t = vtk.vtkTransform()

# finally set to the transform
t.SetMatrix(Rt.ravel().tolist())

# and apply to the camera
camera.ApplyTransform(t)

# set the FoV depending on the camera
camera.SetViewAngle(2.35) # 12 for WAC

Render() # update render

# we might save a screenshot
SaveScreenshot (/path/to/screenshot.png,
ImageQuality=100,
viewOrLayout=view,
TransparentBackground=True,
ImageResolution=(2048, 2048))

```

By computing the contours of the RES field at evenly spaced intervals, which can be easily done in ParaView, it is also possible to obtain three-dimensional traces of the predicted layers (see, as an example, Figure 11.11). These traces do not correspond to any specific layer but can convey the orientation of the layering in different regions of the body in a fairly efficient way. ParaView displays the ellipsoidal model contours on top of the three-dimensional shape model, but producing contour lines overlaid to the actual osiris image (e.g. Figure 11.11e) requires the occlusions generated by the shape of 67P to be correctly taken care of. This operation can be scripted in the following way:

1. The paraview camera orientation, position, and field of view is set as the osiris camera was when the original image was acquired.
2. The screenshot of Figure 11.11a is then saved.
3. The colors of the shape model are changed to red, while the contour lines are colored with a unique black color and a screenshot is saved (Figure 11.11b).
4. The screenshot is processed to create a mask of black pixels (Figure 11.11d).
5. This mask is applied to the first screenshot taken, in order to extract only the contour lines (Figure 11.11c).
6. The extracted image can then be overlaid on the original osiris image (Figure 11.11e).

The 3D shape model (Preusker et al., 2017; Jorda et al., 2016) is the result of processing hundreds of OSIRIS images

to produce a three-dimensional mesh of the surface, and can be used to create additional views of the same scene that can be helpful in correctly understanding the resolved morphological features on the comet surface. Figure 11.12b was created in Blender (e.g. Kent, 2013) to reflect the alteration of terraces and cliffs. Gravitational slopes greater than  $35^\circ$  were used to artificially color the cliffs, while flatter terrains were left in gray by creating an ad-hoc shader. Also, Blender can be easily scripted to align its own camera with the view of any OSIRIS image, as shown in the next script:

```

import bpy
# using transform3d package convert rot mat to
euler angles import transforms3d as tr

render = bpy.context.scene.render
render.resolution_x = 2048
render.resolution_y = 2048
render.resolution_percentage = 100

cc = bpy.data.cameras[0]
cc.sensor_width = 1.35e-02*2048 # pixel size
times number of pixels
cc.sensor_height = 1.35e-02*2048
cc.angle = 2.35 / 180 * np.pi # would be 12 for
WAC

center, Rot = getNacCenterAndRotationAtTime(t)
# as explained above

camera = bpy.context.scene.camera
camera.location = center

# this transform is needed because the camera in
# blender is differently defined in respect to
# NAC/WAC inside spice
Rb = np.array([[0,1,0],[1,0,0],[0,0,-1]])

bpy.context.object.rotation_mode = 'XYZ'
eulers = np.array(tr.euler.mat2euler(Rot.dot(Rb),
'sxyz'))
camera.rotation_euler = eulers

# render the scene to a file
render.filepath = "/path/to/render.png"
bpy.ops.render.render(write_still=True)

```

This script requires the user to correctly set up Blender beforehand by importing the three-dimensional model together with per-vertices gravitational slopes and setting the lighting and the materials as desired. The code can be easily extended to correctly orient the light source to reproduce the observed shadows, as was done in Figure 11.12b, where the shadowing effect was slightly reduced. The complete scripts can be obtained from the author's github page (<https://github.com/luca-penasa>) or by contacting the author.



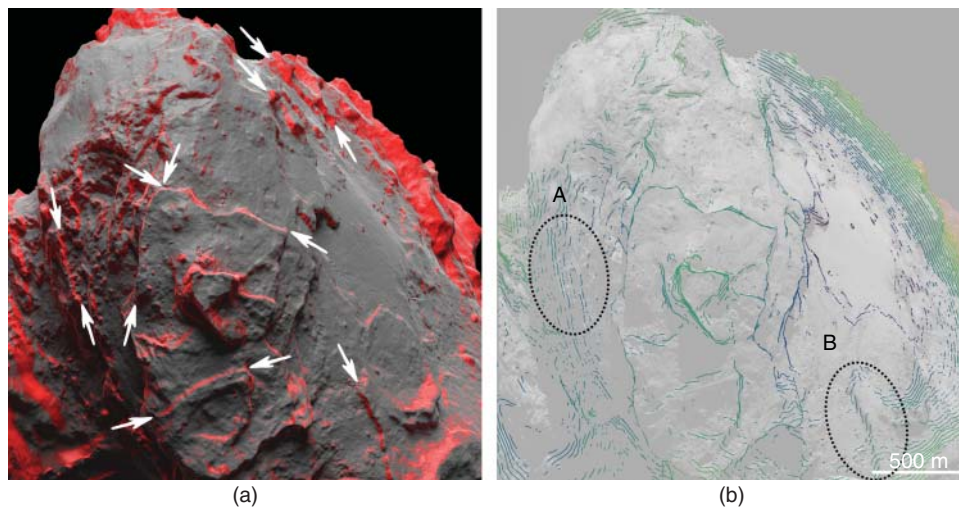


**Figure 11.12** (a) Render of the shape-model made with Blender: the cliffs (regions with gravitational slopes greater than  $35^\circ$ ) were shaded in red to highlight the alternation of cliffs with terraces. White arrows highlight some of the more extended cliffs. The same point of view of the NAC camera was obtained by means of the Python scripts reported in this work. (b) RES contour lines traced only on cliffs to highlight locations where layers are expected to be well exposed. The two ellipses show regions where the model fits the observed cliffs perfectly (A) and where the predicted lines are instead at a slight angle (B).

Figure 11.12 demonstrates the use of the proposed methods as a visual aid for validating the modelling results. The layering of comet Churyumov-Gerasimenko (67P) is documented by the presence of terraces separated by steep cliffs. The cliffs themselves can be easily identified by isolating the regions with a gravitational slope greater than  $35^\circ$ , as shown in Figure 11.12a: cliffs are clearly aligned in strips of terrain displaying lateral continuity. Some of these extended cliffs are highlighted by arrows in Figure 11.12a in order to help the interpretation. The contour lines obtained from the model (Figure 11.12b) are expected to be parallel to the orientation of the cliffs. More comparisons of this kind can be found in Penasa et al. (2017a) and its additional material.

## 11.5 Conclusions

The attempt to reconstruct a 3D model of the layered structure of the lobes of comet 67P is challenged by the scattered observations of the bedding planes. This issue was tackled by a very simple modelling strategy based on the approximation of the layers as shapes derived from analytical functions (spheres or ellipsoids). The implementation of the solver was required to take into account the rotational symmetry of the ellipsoids and to correctly devise a strategy for the initialization of the model parameters. We found that convergence between model and observations for 67P was robust to random initialization of the parameters. The described approach

has the advantage of providing a small set of parameters with a precise physical meaning whose standard errors can be easily determined by using a bootstrap strategy. These errors made it possible to compare the *center* of the concentric layering (the center of the ellipsoidal model) with the center of mass of the respective lobe from a statistical point of view, demonstrating that the two points do not correspond.

The proposed modelling strategy was implemented *outside* commercial 3D geomodelling platforms and required the development of ad-hoc visualization strategies useful for comparing the results with the morphological features that could be observed from osiris images.

We stress that the modelling of the layers of 67P lobes through ellipsoids is a simplification of a more complex shape whose further investigation will require improvements able to take into account higher complexity.

## Acknowledgments

OSIRIS was built by a consortium of the Max-Planck-Institut für Sonnensystemforschung in Göttingen, Germany, CISAS-University of Padova, Italy, the Laboratoire d'Astrophysique de Marseille, France, the Instituto de Astrofísica de Andalucía, CSIC, Granada, Spain, the Research and Scientific Support Department of the European Space Agency, Noordwijk, The Netherlands, the Instituto Nacional de Técnica Aeroespacial, Madrid, Spain, the Universidad Politécnica de Madrid, Spain,



the Department of Physics and Astronomy of Uppsala University, Sweden, and the Institut für Datentechnik und Kommunikationsnetze der Technischen Universität Braunschweig, Germany. The support of the national funding agencies of Germany (DLR), Italy (ASI), France

(CNES), Spain (MEC), Sweden (SNSB), and the ESA Technical Directorate is gratefully acknowledged. We thank the ESA teams at ESAC, ESOC, and ESTEC for their work in support of the Rosetta mission.

## References

- Acton, C., Bachman, N., Semenov, B., and Wright, E. (2018). A look towards the future in the handling of space science mission geometry. *Planetary and Space Science* 150: 9–12. doi: 10.1016/j.pss.2017.02.013.
- Agarwal, S., Mierle, K., and Others (2016). Ceres solver, <http://ceres-solver.org>.
- Annex, A., Carcich, B., McAuliffe, J. et al. (2017). *Andrewannex/Spiceypy: Spiceypy* 2.1.0. doi: 10.5281/zenodo.1044745.
- Auger, A.-T., Groussin, O., Jorda, L. et al. (2017). Meter-scale thermal contraction crack polygons on the nucleus of comet 67P/Churyumov-Gerasimenko. *Icarus*. doi: 10.1016/j.icarus.2017.09.037.
- Basilevsky, A., Mall, U., Keller, H. et al. (2017). Geologic analysis of the Rosetta NavCam, Osiris and ROLIS images of the comet 67P/Churyumov-Gerasimenko nucleus. *Planetary and Space Science* 137: 1–19. doi:10.1016/j.pss.2017.01.002.
- Birch, S.P.D., Tang, Y., Hayes, A.G. et al. (2017). Geomorphology of comet 67P/Churyumov-Gerasimenko. *Monthly Notices of the Royal Astronomical Society* 469 (Suppl. 2): S50–S67. doi: 10.1093/mnras/stx1096.
- Bistacchi, A., Massironi, M., Dal Piaz, G.V. et al. (2008). 3D fold and fault reconstruction with an uncertainty model: An example from an Alpine tunnel case study. *Computers and Geosciences* 34 (4): 351–372. doi: 10.1016/j.cageo.2007.04.002.
- Calcagno, P., Chilès, J., Courrioux, G., and Guillen, A. (2008). Geological modelling from field data and geological knowledge. *Physics of the Earth and Planetary Interiors* 171 (1–4): 147–157. doi: 10.1016/j.pepi.2008.06.013.
- Caumon, G., Collon-Drouaillet, P., Carlier, L. et al. (2009). Surface-based 3D modeling of geological structures. *Mathematical Geosciences* 41 (8): 927–945. doi: 10.1007/s11004-009-9244-2.
- Caumon, G., Gray, G., Antoine, C., and Titeux, M.-O. (2013). Three-dimensional implicit stratigraphic model building from remote sensing data on tetrahedral meshes: Theory and application to a regional model of La Popa Basin, NE Mexico. *IEEE Transactions on Geoscience and Remote Sensing* 51 (3): 1613–1621. doi: 10.1109/TGRS.2012.2207727.
- Chernick, M.R. (2008). *Bootstrap Methods: A Guide for Practitioners and Researchers*, Wiley Series in Probability and Statistics, 2nd edn., Wiley-Interscience, Hoboken, N.J.
- Cignoni, P., Callieri, M., Corsini, M. et al. (2008). MeshLab: An open-source mesh processing tool. In: *Eurographics Italian Chapter Conference* (ed. V. Scarano, R.D. Chiara and U. Erra). The Eurographics Association doi: 10.2312/LocalChapterEvents/ItalChap/ItalianChapConf2008/129-136.
- Eberly, D. (2013). Distance from a point to an ellipse, an ellipsoid, or a hyperellipsoid. <https://www.geometrictools.com/Documentation/DistancePointEllipseEllipsoid.pdf>.
- Efron, B. (1979). Bootstrap methods: Another look at the jackknife. *The Annals of Statistics* 7 (1): 1–26. doi: 10.2307/2958830.
- El-Maarry, M.R., Thomas, N., Giacomini, L. et al. (2015a). Regional surface morphology of comet 67P/Churyumov-Gerasimenko from Rosetta/OSIRIS images. *Astronomy and Astrophysics* 583: A26. doi: 10.1051/0004-6361/201525723.
- El-Maarry, M.R., Thomas, N., Gracia-Berná, A. et al. (2015b). Fractures on comet 67P/Churyumov-Gerasimenko observed by Rosetta/OSIRIS. *Geophysical Research Letters* 42 (13): 5170–5178. doi: 10.1002/2015GL064500.
- El-Maarry, M.R., Thomas, N., Gracia-Berná, A. et al. (2016). Regional surface morphology of comet 67P/Churyumov-Gerasimenko from Rosetta/OSIRIS images: The southern hemisphere. *Astronomy and Astrophysics* 593: A110. doi: 10.1051/0004-6361/201628634.
- Fernández, O. (2005). Obtaining a best fitting plane through 3D georeferenced data. *Journal of Structural Geology* 27 (5): 855–858.
- Fisher, N.I. (1993). *Statistical Analysis of Circular Data*. Cambridge University Press, Cambridge, England and New York, USA.
- Fornasier, S., Hasselmann, P.H., Barucci, M.A. et al. (2015). Spectrophotometric properties of the nucleus of comet 67P/Churyumov-Gerasimenko from the OSIRIS instrument onboard the ROSETTA spacecraft. *Astronomy and Astrophysics* 583: A30. doi: 10.1051/0004-6361/201525901.
- Franceschi, M., Penasa, L., Massironi, M. et al. (2020). Global-scale brittle plastic rheology at the cometesimals merging of comet 67P/Churyumov-Gerasimenko. In:

- Proceedings of the National Academy of Sciences*, 201914552. doi: 10.1073/pnas.1914552117.
- Giacomini, L., Massironi, M., El-Maarry, M.R. et al. (2016). Geologic mapping of the Comet 67P/Churyumov–Gerasimenko’s Northern hemisphere. *Monthly Notices of the Royal Astronomical Society* 462 (Suppl. 1): S352–S367. doi: 10.1093/mnras/stw2848.
- Grose, L., Ailleres, L., Laurent, G., and Jessell, M. (2021). LoopStructural 1.0: Time-aware geological modelling. *Geoscientific Model Development* 14 (6): 3915–3937. doi: 10.5194/gmd-14-3915-2021.
- Guilbert-Lepoutre, A., Besse, S., Mousis, O. et al. (2015). On the evolution of comets. *Space Science Reviews* 197 (1–4): 271–296. doi:10.1007/s11214-015-0148-9.
- Hardy, R.L. (1990). Theory and applications of the multiquadric-biharmonic method 20 years of discovery 1968–1988. *Computers and Mathematics with Applications* 19 (8–9): 163–208.
- Hillier, M.J., Schetselaar, E.M., de Kemp, E.A., and Perron, G. (2014). Three-dimensional modelling of geological surfaces using generalized interpolation with radial basis functions. *Mathematical Geosciences* 46 (8): 931–953. doi: 10.1007/s11004-014-9540-3.
- Jorda, L., Gaskell, R., Capanna, C. et al. (2016). The global shape, density and rotation of Comet 67P/Churyumov-Gerasimenko from preperihelion Rosetta/OSIRIS observations. *Icarus* 277: 257–278. doi: 10.1016/j.icarus.2016.05.002.
- Keller, H.U., Barbieri, C., Lamy, P. et al. (2007). OSIRIS – The Scientific Camera System Onboard Rosetta. *Space Science Reviews* 128 (1–4): 433–506. doi: 10.1007/s11214-006-9128-4.
- Keller, H.U., Mottola, S., Davidsson, B. et al. (2015). Insolation, erosion, and morphology of comet 67P/Churyumov–Gerasimenko. *Astronomy and Astrophysics* 583: A34. doi: 10.1051/0004-6361/201525964.
- Kent, B.R. (2013). Visualizing astronomical data with Blender. *Publications of the Astronomical Society of the Pacific* 125 (928): 731.
- Laurent, G. (2016). Iterative thickness regularization of stratigraphic layers in discrete implicit modeling. *Mathematical Geosciences* 48 (7): 811–833. doi: 10.1007/s11004-016-9637-y.
- Lee, J.-C., Massironi, M., Ip, W.-H. et al. (2016). Geomorphological mapping of comet 67P/Churyumov–Gerasimenko’s Southern Hemisphere. *Monthly Notices of the Royal Astronomical Society* 462 (Suppl. 1): S573–S592. doi: 10.1093/mnras/stx450.
- Massironi, M., Simioni, E., Marzari, F. et al. (2015). Two independent and primitive envelopes of the bilobate nucleus of comet 67P. *Nature* 526 (7573): 402–405. doi: 10.1038/nature15511.
- Oklay, N., Vincent, J.-B., Fornasier, S. et al. (2016). Variegation of comet 67P/Churyumov-Gerasimenko in regions showing activity. *Astronomy & Astrophysics* 586: A80. doi:10.1051/0004-6361/201527369.
- Pajola, M., Oklay, N., La Forgia, F. et al. (2016). Aswan site on comet 67P/Churyumov–Gerasimenko: Morphology, boulder evolution, and spectrophotometry. *Astronomy and Astrophysics* 592: A69. doi: 10.1051/0004-6361/201527865.
- Penasa, L., Massironi, M., Naletto, G. et al. (2017a). A three-dimensional modelling of the layered structure of comet 67P/Churyumov–Gerasimenko. *Monthly Notices of the Royal Astronomical Society* 469 (Suppl. 2): S741–S754. doi: 10.1093/mnras/stx2899.
- Penasa, L., Massironi, M., Ferrari, S. et al. (2017b). The layered structure of the nucleus of the comet 67P: Implications on missing volumes and lobes orientations. *In European Planetary Science Congress 11*: pp. EPSC2017–485.
- Preusker, F., Scholten, F., Matz, K.-D. et al. (2017). The global meter-level shape model of comet 67P/Churyumov–Gerasimenko. *Astronomy and Astrophysics* 607: L1. http://doi: 10.1051/0004-6361/201731798.
- Rickman, H., Marchi, S., A’Hearn, M.F. et al. (2015). Comet 67P/Churyumov–Gerasimenko: Constraints on its origin from OSIRIS observations. *Astronomy and Astrophysics* 583: A44. doi: 10.1051/0004-6361/201526093.
- Rolo, R.M., Radtke, R., and Costa, J.F.C.L. (2017). Signed distance function implicit geologic modeling, *REM – International. Engineering Journal* 70 (2): 221–229. doi: 10.1590/0370-44672016700146.
- Ruzicka, B.-K., Penasa, L., Boehnhardt, H. et al. (2019). Analysis of layering-related linear features on comet 67P/Churyumov–Gerasimenko. *Monthly Notices of the Royal Astronomical Society* 482 (4): 5007–5011. doi: 10.1093/mnras/sty3079.
- Schiavo, A., Dal Piaz, G.V., Monopoli, B. et al. (2015). Geology of the Brenner Pass–Fortezza Transect, Italian Eastern Alps. *Journal of Maps* 11 (1): 201–215. doi: 10.1080/17445647.2014.980337.
- Schroeder, W., Martin, K., and Lorensen, B. (2006). *The Visualization Toolkit: An Object-Oriented Approach to 3D Graphics; Visualize Data in 3D – Medical, Engineering or Scientific; Build Your Own Applications with C++, Tcl, Java or Python; Includes Source Code for VTK (Supports Unix, Windows and Mac)*, 4th edn. Kitware, Inc., Clifton Park, NY.
- Sierks, H., Barbieri, C., Lamy, P.L. et al. (2015). On the nucleus structure and activity of comet

- 67P/Churyumov–Gerasimenko. *Science* 347 (6220):  
aaa1044.
- Squillacote, A.H., Ahrens, J., Law, C. et al. (2007).  
*The Paraview Guide* 366: Kitware.
- Thomas, N., Sierks, H., Barbieri, C. et al. (2015). The  
morphological diversity of comet 67P/Churyumov–  
Gerasimenko. *Science* 347 (6220) aaa0440–aaa0440:  
doi: 10.1126/science.aaa0440.
- Vincent, J.-B., Hviid, S.F., Mottola, S. et al. (2017). Constraints  
on cometary surface evolution derived from a statistical  
analysis of 67P’s topography. *Monthly Notices of the Royal  
Astronomical Society* 469 (Suppl. 2): S329–S338. doi: 10  
.1093/mnras/stx1691.